Decisive Role of Spin-States and Spin-Coupling in Dictating Selective O_2 Adsorption in Chromium(II) Metal-Organic Framework

Reshma Jose[a], Srinivasu Kancharlapalli[b], Tapan K Ghanty[b#], Sourav Pal*[c] and Gopalan Rajaraman*[a]

a) Department of Chemistry, Indian Institute of Technology Bombay, Powai, Mumbai-400076, India. Tel: (+91)-22-2576-7183. Email: rajaraman@chem.iitb.ac.in

b)Theoretical Chemistry Section, Bhabha Atomic Research Centre, Mumbai-400085, India. Email: srinu.barc@gmail.com, tapang@barc.gov.in. #Present address: Bio-Science Group, Bhabha Atomic Research Centre, Mumbai-400085, India.

c) Department of Chemistry, Indian Institute of Science Education and Research, Kolkata, Mohanpur, Nadia – 741246, India. Email: s.pal@iiserkol.ac.in

Abstract: Coordinatively unsaturated Chromium (II)-based $Cr_3[(Cr_4Cl)_3(BTT)_8]_2$ (Cr-BTT; BTT^{3-}=1,3,5-benzenetristetrazolate) metal-organic framework (MOF) has been shown to exhibit exceptional selectivity towards adsorption of O_2 over N_2/H_2. Using periodic Density Functional Theory (DFT) calculations, we attempt to decipher the origin of this puzzling selectivity. By computing and analyzing the magnetic exchange coupling, binding energies, the partial density of states (pDOS), and adsorption isotherms for the pristine and gas bound MOFs $[(Cr_4(X)_4Cl)_3(BTT)_8]^{3-}$ (X=O_2, N_2, and H_2), we unequivocally establish the role of spin-states and spin-coupling in controlling the gas selectivity. The computed geometries and gas adsorption isotherms are consistent with the earlier experiments. The O_2 binding to the MOF follows an electron-transfer mechanism resulting in a Cr(III) superoxo species ($O_2^{-\bullet}$) with a very strong antiferromagnetic coupling between the two centers, while N_2/H_2 found to weakly interact with the metal centre and hence only slightly perturb the associated coupling constants. Although the gas bound and unbound MOFs have S =0 ground state (GS), the nature of spin configurations and the associated magnetic exchanges are dramatically different. The binding energy and the number of oxygen molecules that can favorably bind to the Cr center were found to vary with respect to the spin-state with a significant energy margin (47.6 kJ/mol). This study offers a hitherto unknown strategy of utilizing spin-state/spin-couplings to control gas adsorption selectivity in MOFs.

Introduction

Metal Organic Frameworks (MOFs), owing to their fascinating properties such as structural and functional diversity, tunable pore size, and enormous surface area, have tremendous applications in gas storage[1], molecular separation[2], sensors[3], and catalysis.[4] Though zeolites, covalent organic frameworks, and complex hydrides are available for gas separation applications[5], MOF based separative systems have attracted wide attention due to their high selectivity as a result of their extensive chemical diversity and porous nature in comparison to other classical adsorbate systems.[6] The microporous nature of the MOFs enables systematic immobilization of the functional materials and are envisaged as a practical promise for gas purification and separation applications at an industrial scale. Whilst several MOFs based on first-row transition metals are known for switchable magnetic characteristics under the influence of guest molecule[7], temperature[8], and pressure,[9] there are only a few reports on high selectivity towards oxygen. The selective adsorption of oxygen over other gases that generate high purity oxygen (> 99%) has applications in healthcare, oxy-fuel combustion[10], ozone generation, semiconductors and other industries. This is a challenging task, as the separation of O_2 from the N_2 mixture is a hassle due to the similarity in their physical properties[11], such as kinetic diameter, polarizability, boiling point, etc. The current industry standard is cryogenic separation, which demands high pressure, temperature and large infrastructure that escalate production costs. Thus, an alternative separation technique based on porous material is in high demand. Long et al. recently reported $Cr_3[(Cr_4Cl)_3(BTT)_8]_2$ (BTT^{3-} =1,3,5-benzenetristetrazolate)[12] MOF, which exhibits very high selectivity for oxygen over hydrogen and nitrogen. Despite the structural similarity of this MOF to other metal ion MOFs reported, this shows high selectivity towards O_2 compared to N_2 and is currently one among the best MOFs for O_2 selective separations.[12] While multiple factors can influence gas adsorption in MOFs, the origin of very high selectivity for O_2 is perplexing because structurally similar metal ion MOFs are unselective. Though the role of spin state and spin coupling in selective gas binding is not well studied in MOFs, there are reports on the magnetic separation of small molecules.[13] The spin states-based selectivity of gas in MOF[14] needs to be addressed in detail.

Computational details

All calculations were carried out using periodic Density Functional Methods[15] implemented in the CP2k 2.4.0 suite. The Perdew−Burke−Ernzerhof (PBE)[16] gradient-corrected, generalized gradient approximation (GGA) was used to describe the exchange−correlation functional, and DZVP-MOLOPT-GTH (valence double zeta (ζ) plus polarization, molecularly optimized, Goedecker-Teter-Hutter) basis set for atoms (H, C, O, N, Cl) and DZVP-MOLOPT-SR-GTH for Chromium atom by incorporating the short-range forces with gaussian augmented plane wave (GAPW) approach with a kinetic energy cutoff of 400 Ry. The Grimme's D2 correction (DFT-D2) was used to account for the dispersion interactions. We have also performed calculations using D3 dispersion correction, which yields very similar geometries, binding energies, and *J* values (see Table S1). The boundary conditions a=b=c, which is set as 18.6695 Å.[17] Our earlier studies on [Mn_{19}] cluster reveal that the combination of PBE with plane-wave basis sets yields *J* values which are similar to the estimate obtained from B3LYP employing Gaussian type basis set. The PBE functional with the plane-wave basis set is shown to offer less delocalization, perhaps due to confinement, and this improves the numerical estimate of *J* compared to hybrid B3LYP functional. This benchmark established by Ruiz et al. and also by us earlier offers confidence in the methodology chosen.[17-18] Adsorption isotherms were simulated through the Grand Canonical Monte Carlo technique as implemented in the RASPA software.[19] The Lennard−Jones (LJ) parameters for the considered framework atoms were taken from Universal Force Field (UFF),[20], and Lorentz–Berthelot mixing rules are used to calculate the cross interactions. Both N_2 and O_2 molecules were modeled using the TraPPE force field.[21] We used 50,000 equilibration cycles and 50,000 production cycles for each simulation and considered insertion, deletion, translation, and rotation moves. Since the chemisorption of O_2 cannot be modeled using the GCMC technique, we considered initial framework structures with the different number of O_2 molecules chemisorbed, and the corresponding weight of O_2 is also considered for plotting the O_2 loading in addition to the loading obtained from the GCMC simulations.

Results and Discussion

In this work, we have undertaken detailed periodic DFT calculations[16] to decipher the origin of the selectivity observed starting from the X-ray structure reported[12] (Figure 1(a)). This methodology has proven to yield very good geometries for open-shell MOFs and has shown to yield a good numerical estimate of exchange coupling constants (*J*).[22] We have optimized the geometry of $[(Cr_4Cl)_3(BTT)_8]^{3-}$ species and then consider oxygen adsorption in each of the Cr site leading to $[(Cr_4(O_2)_4Cl)_3(BTT)_8]^{3-}$ species where end-on Cr(III)-$O_2^{-\bullet}$ superoxo species is formed. The calculations on the O_2 bound MOF ($[(Cr_4(O_2)_4Cl)_3(BTT)_8]^{3-}$) yields the Cr-O, O-O distances and Cr-O-O angles as 1.815 Å, 1.283 Å and 125.7°, respectively and this is in excellent agreement with neutron diffraction data of 1.84(±2) Å, 1.26(±2) Å and 129° (±2)) reported. A shorter Cr-O distance found here in the end-on Cr(III)-$O_2^{\bullet-}$ superoxo MOF structure suggests less steric crowding compare to the end-on Cr(III)-$O_2^{\bullet-}$ superoxo biomimic model reported where the computed Cr-O distances are distinctly longer (1.965 Å).[23] The topological structure of $[(Cr_4Cl)_3(BTT)_8]^{3-}$ MOF has three Js[24] (see Figure 1(a)) with J_1 describing the interaction between two Cr(II) centers mediated via a BTT/μ_4-Cl bridges and J_2 via the μ_4-Cl bridge and J_3 between two {Cr_4} tetrameric units via the BTT ligands. For the $[(Cr_4(O_2)_4Cl)_3(BTT)_8]^{3-}$ species, there is also an additional exchange between Cr(III) and the $O_2^{\bullet-}$ superoxo species (J_4). Periodic DFT calculations for $[(Cr_4Cl)_3(BTT)_8]^3$ ($[(Cr_4(O_2)_4Cl)_3(BTT)_8]^3$) yield J_1=-25.8 (-23.8) cm^{-1}, J_2= -41.8 (+3.4) cm^{-1} and J_3 = 0.3 (+0.5) cm^{-1} (J_4 = -1366 cm^{-1}) with computed error in *Js* being negligible (Sees Table S2). Computed O-O stretching frequencies on a $[(Cr_4Cl)_3(BTT)_8]^{3-}$ model is consistent with experiments (1206 cm^{-1} vs. 1193 cm^{-1}).[12] For the unbound MOF, the antiferromagnetic J_2 is the strongest, followed by J_1 and weakly ferromagnetic J_3, and this trend is in line with the available magneto-structural correlations.[24-25] The pseudo-Jahn-Teller elongation along the Cr-Cl bond results in dominant $d_z^2|p_z|d_z^2$ overlap leading to a strong antiferromagnetic coupling. The J_3 interaction is mediated via longer tetrazolate bridges, and hence it is relatively weak.

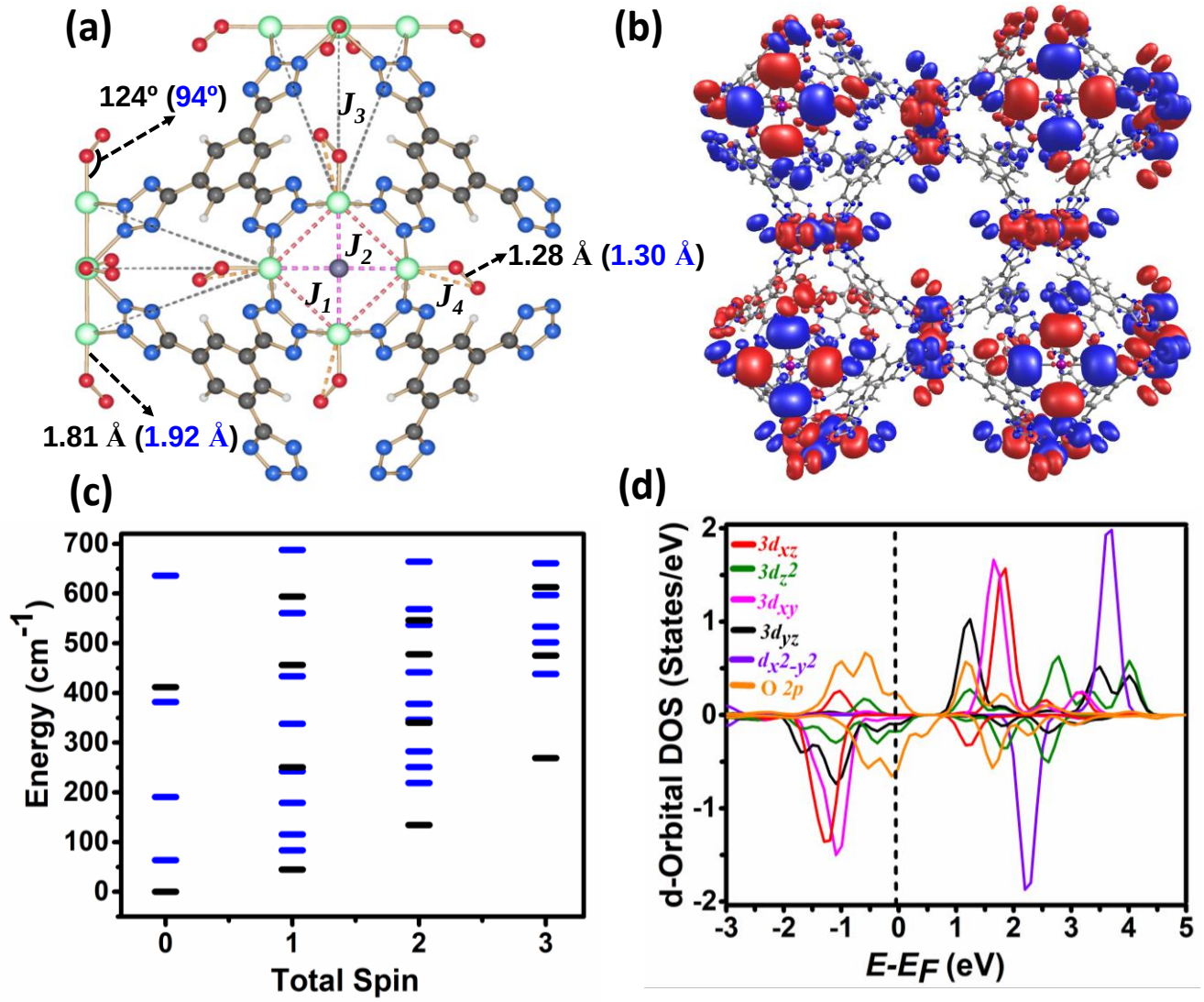

Figure 1. (a) Geometry and representation of $J_{1\text{-}4}$, bond parameters of GS (in black) and HS in $[(Cr_4(O_2)_4Cl)_3(BTT)_8]^{3-}$ MOF. (Cr-green, Cl-purple, N-blue, C-grey, H-white) **(b)** GS spin density plot of $[(Cr_4(O_2)_4Cl)_3(BTT)_8]^3$. **(c)** Estimated spin-state ladder based on DFT *J*s for O_2 bound (black) and unbound MOF. **(d)** The d-orbital DOS plot for $[(Cr_4(O_2)_4Cl)_3(BTT)_8]^{3-}$ MOF.

This set of *J* values yield S = 0 ground state (GS) for {Cr_4} unit with another S =0 and S = 1 excited states at 63.6 and 83. 6 cm^{-1} higher, respectively, suggesting competing for AF interactions (see Figure 1(c)). Calculations yield two-spin-up-two-spin-down Cr^{II} center as the lowest energy spin configuration (Figure 1(b)) among all the spin configurations computed. For O_2 bound MOF, all *J*s except J_2 and J_3 are estimated to be antiferromagnetic, with J_4 being the strongest, and this is also consistent with experiments.[23, 26] The Cr(III) with unpaired electrons in d_{xy}, $d_{xz,}$ and d_{yz} orbitals do not offer a direct overlap with the linear Cr-Cl-Cr bridge resulting in weak ferromagnetic J_2 exchange. Strong antiferromagnetic J_1 and J_4 enforces S =0 GS with alternate spin-up and down in the {Cr_4} unit with the $O_2^{\bullet-}$ spin antiferromagnetically coupled to each Cr center (see Figure S1 in ESI), and this configuration is different from unbound MOF S = 0 state. The unpaired electrons are found to be in the O-O (p*) orbital with the distal oxygen found to have significant radical character (0.6), with the total unpaired electrons of ~0.93 detected on the oxygen molecule revealing a strong superoxo character. The nonlinear Cr-O-O angle of 126° facilitates strong overlap with the $\sigma^*(d_z^2)$ and the axial π-donor Cl orbital destabilize the $d_{xz/yz}$ orbitals leading to, stronger overlap and hence strong binding as shown in the qualitative MO diagram derived (see Figure 2).

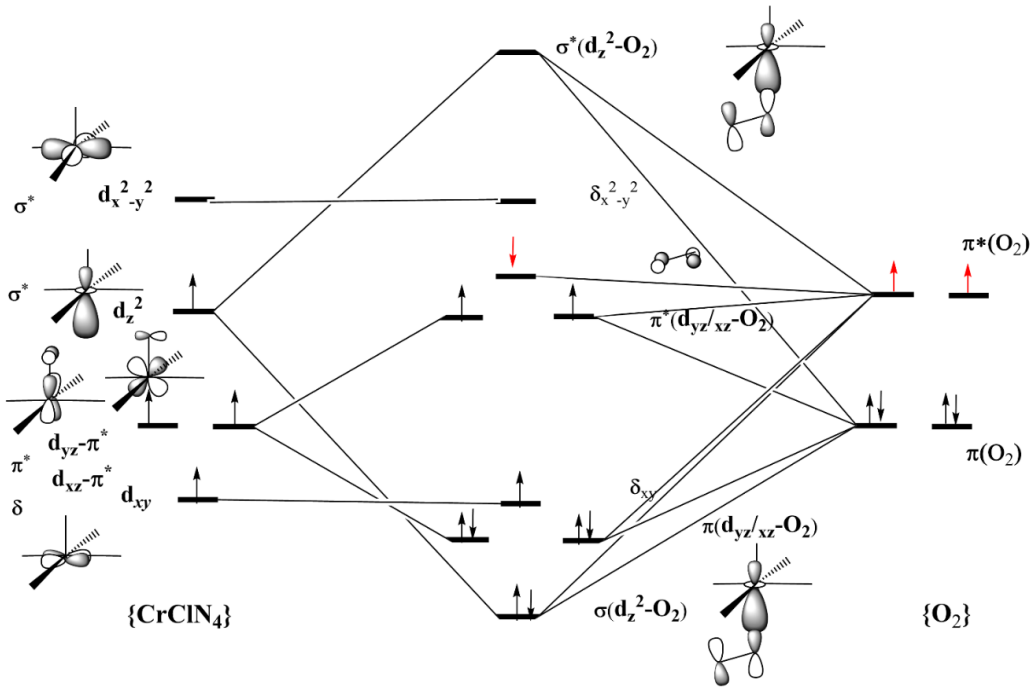

Figure 2. The qualitative Molecular Orbital Diagram showing the interaction of O_2 with the Chromium center.

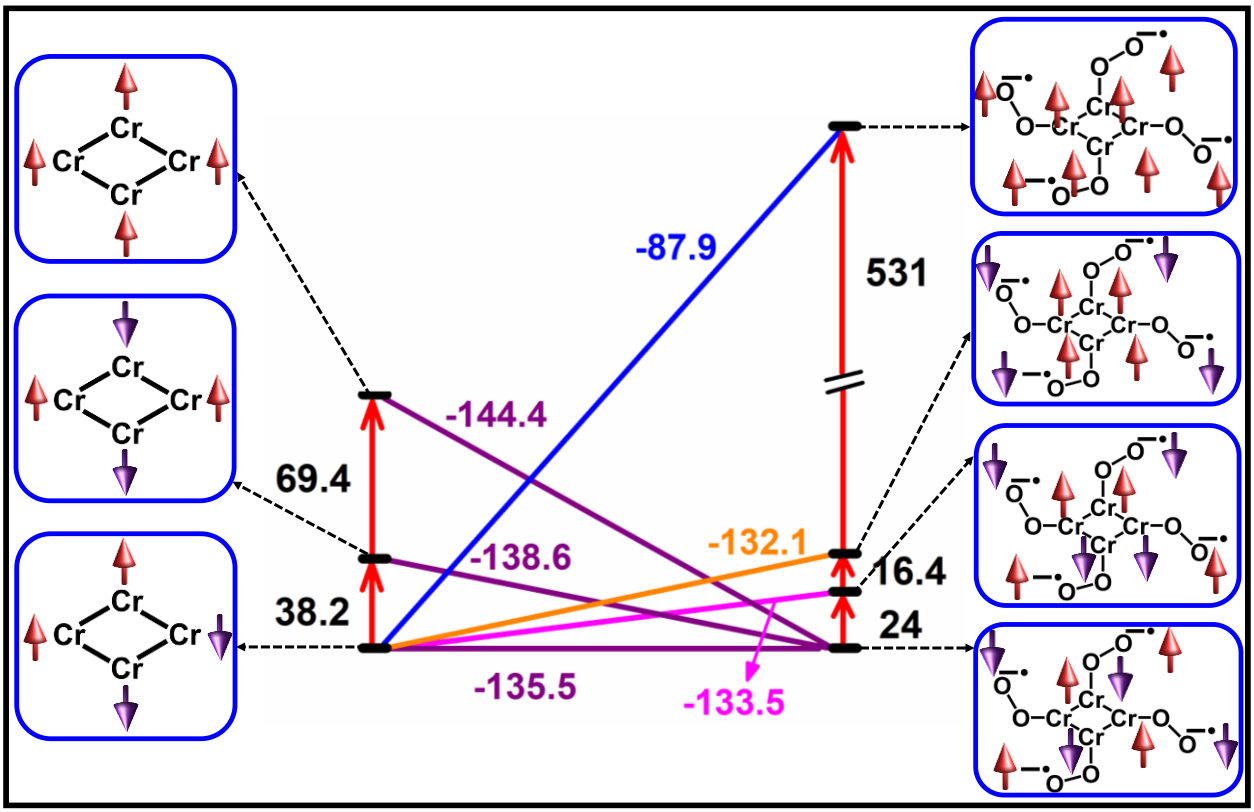

Figure 3. The energy level diagram depicts different spin states' comparative energies before and after oxygen binding (in kJ/mol).

The oxygen-binding was analyzed by the pDOS plot (Figure 1d), and near the Fermi level, the oxygen p-orbitals are found to mix strongly with the d-based orbitals of Cr ions. Particularly the $d_{x^2-y^2}$, and d_{z^2} orbitals are found close to the Fermi level, and if we compare the pDOS with unbound MOF (see Figure 5a), reduction in the Cr d-orbital density is visible, suggesting oxidation of Cr ion as expected. Additionally, both the d_{z^2} and d_{yz} orbitals of Cr ions are found to split near the Fermi level suggesting mixing of these orbitals with oxygen leading to bonding/anti-bonding combinations as described in the qualitative MO diagram (see Figure 2). The binding energy (BE) computed by comparing the GS energy of $[(Cr_4Cl)_3(BTT)_8]^{3-}$ and $[(Cr_4(O_2)_4Cl)_3(BTT)_8]^{3-}$ in Cr(III)-$O_2^{\bullet-}$ mode of binding is estimated to be -136.7 kJ/mol (per Chromium site).

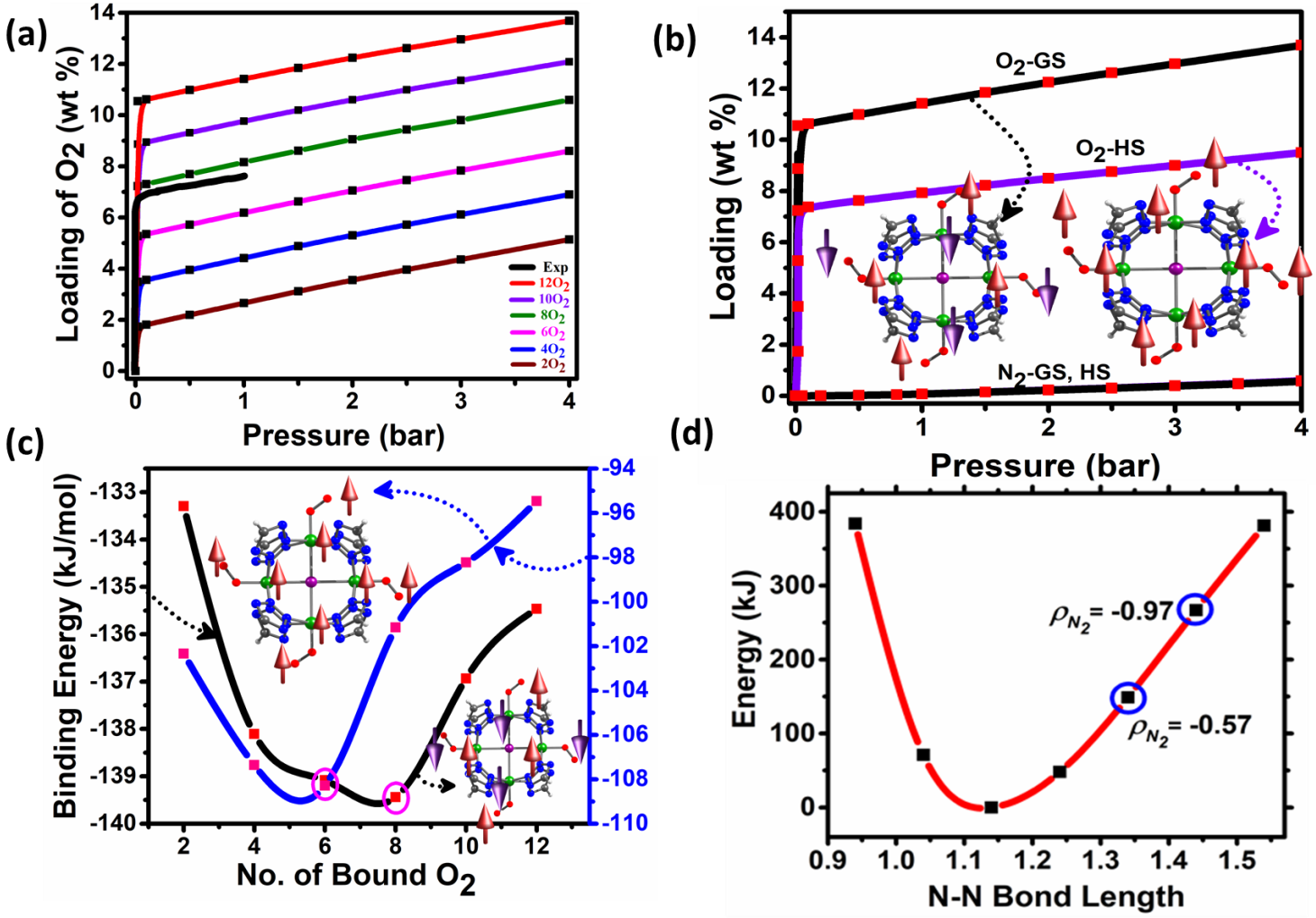

Figure 4. (a) Computed adsorption isotherm for successive O_2 binding (**b**) Comparative adsorption isotherm for O_2 and N_2 in GS and HS state(**c**) Computed BE for successive addition of oxygen in GS (black line, S=0) and HS state (blue line).d) The rigid scan of N-N bond distance in N_2 bound MOF. Here the blue circled region indicates the formation of radical at the N2 moitetyand corresponding spin density.

This large exothermicity computed reveals the favorable formation of end-on Cr(III)-$O_2^{\bullet-}$ superoxo species.[12] The BE reported by us for a well characterized Cr(III)-$O_2^{\bullet-}$ superoxo species [Cr(14-TMC)(OO)(Cl)]$^+$ is -77 kJ/mol, which is significantly smaller compared to MOFs.[23, 26] In both cases, the -Cl ligand is found to be in the *trans* position, unveiling the importance of π-donor ligands in the stability of such transient species.[27] To understand the role of spin-state in gas-binding, we computed the BE for various spin-ladders estimated from the exchange interactions. If a higher excited S =0 state is considered, the BE is found to differ by a few kJ/mol (see Figure 3). For the high-spin (HS) state, the BE is relatively unfavorable (-87.9 kJ/mol per site with respect to the GS), and this is 47.6 kJ/mol (per site) higher compared to the GS, suggesting strong dependency of binding energy with respect to the spin states. The O_2 adsorption isotherm experimentally reported reveals that it is extraordinarily steep, reaching 7.01 wt% at 0.2 bar and saturates at 7.56 wt% at 1 bar, which is smaller than 11.3 wt% expected if all Cr ions are bound to O_2. This approximately translates to O_2 binding in eight Cr centers among the 12 ions present in our adapted unit cell. In order to check the difference in BE with respect to the number of oxygen molecules to see if a cooperative binding is present, we estimated BE by varying the number of O_2 molecules from 2 (leaving ten chromium sites vacant) to 12. As we go from 2 to 8 (~6.3 kJ per site), BE becomes larger and larger, with the largest per site BE noted for eight oxygen molecules (-139.4 kJ/mol). The addition of further oxygen molecules tends to decrease the BE (2.5 kJ/mol per site), suggesting that 10 or 12 oxygen (full saturation point) binding is not very favorable, and this is consistent with experiments. The addition of oxygen beyond eight units tends to increase the steric crowding at the tetrameric binding sites and also demands oxidation of all the Cr^{II} to Cr^{III} at the tetrameric unit cell. Both of which has a larger energy penalty, diminishing the binding energy.

For the HS state, different behavior is noted, with the most favorable BE found for six O_2 molecules with a much steeper energy penalty for additional oxygen bindings (12.8 kJ/mol per site). Again, spin-state was found to dictate not only the BE preferences but also the number of oxygen molecules that can bind to the MOF in a favorable manner (see Figure 4c). This suggests that switching of the spin-state/exchange coupling is therefore expected to influence the selectivity considerably. To further understand the binding of oxygen, we have simulated the adsorption isotherms at 298 K and 0-4 bar using the RASPA suite (see Figure 4(a, b) and computational details). To account for Cr-O covalent bond formation and BE difference among various spin-

states, we have performed further adsorption isotherm calculations using the starting geometry of $[(Cr_4Cl)_3(O_2)_n(BTT)_8]^{3-}$ (n=2, 4, 6, 8, 10 and 12, (see Figure 4(a), see ESI for the corresponding equation used). The GS electronic configuration isotherm is very similar to the experimental curve.[12] Moreover, from the simulated curve, it is clear that the HS state has a lesser tendency to bind oxygen compared to the antiferromagnetic S = 0 GS, unveiling a strong spin-state dependent O_2 loading feature. The reason for unfavorable gas binding in the HS state (S= 8 for a tetrameric Cr(III)-$O_2^{\bullet-}$ unit) is partially due to the strong antiferromagnetic exchange between Cr(III) and $O_2^{\bullet-}$ unit (J_4 value is ~16.3 kJ/mol) and also due to unfavorable structural deformation in the HS state where the Cr(III)-O as well as O-O bonds are much longer compared to the low-spin GS configuration (see Figure 1(a)).

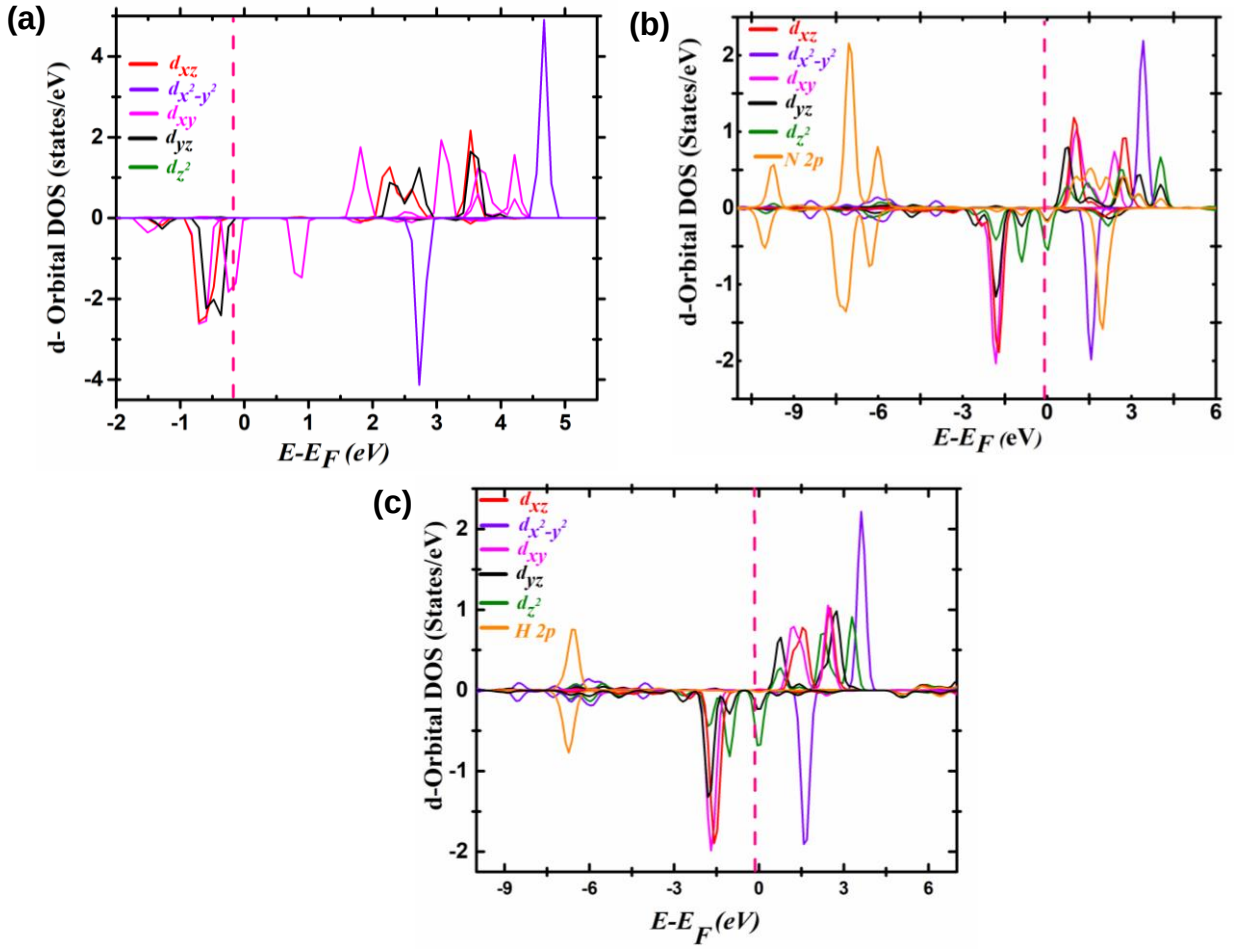

Figure 5. The d orbital DOS for (a) unbound MOF (b) the N_2 bound MOF (c) H_2 bound MOF, where Fermi energy level is marked with pink dotted lines.

Further calculations were performed for N_2 and H_2 adsorption, which yields BE of -35 kJ/mol and -16 kJ/mol, respectively. Both the values are significantly smaller than that found for O_2, rationalizing the extraordinary selectivity for O_2 observed experimentally for this MOF. The binding of N_2/H_2 results in an S = 0 GS similar to that of unbound MOF. The *J* values for MOF-N_2 (MOF-H_2) are estimated to be J_1= -23.4 (-27.3) cm^{-1}, J_2 = -34.1 (-46.6) cm^{-1}, J_3= -0.6 (0.63) cm^{-1}, suggesting dominant antiferromagnetic coupling leading to a diamagnetic GS at lower temperatures. The N_2 is found to bind on end-on fashion with an estimated Cr-N distance of 2.19 Å while the H_2 binds in a side-on fashion with an average Cr-H distance of 2.53 Å with the Cr-H-H angle ~ 81º suggesting a weak overlap with the metal ion and this is also reaffirmed in the pDOS plot (see Figure 5) where a very little overlap of Cr d-orbitals with the N_2/H_2 p-orbitals is noted. If we compare the d-based orbitals of Cr ion in the presence and absence of N_2/H_2 binding, it is clear that the d_z^2 orbital is split, suggesting a weak Cr(II)…N_2/H_2 interaction with this orbital. To assess the energetic cost associated with the formation of {Cr(III)-$N_2^{-\bullet}$} similar in line with oxygen binding, a coordinate scan analysis was performed by varying the N…N bond from 0.94 Å to 1.54 Å. This reveals a partial formation of Cr(III)-$N_2^{-\bullet}$ species at N-N~1.34 Å, with an energy penalty of ~150 kJ/mol (per site), revealing the reason for very high selectivity towards O_2 (see Figure 4d). Unlike O_2, the isotherm obtained for N_2 shows a similar binding trend for HS and S=0 GS, suggesting that spin-state dependency in N_2 is absent (Figure 4(b)). A similar trend is also visible for the H_2 binding, unveiling the reason for the very high selectivity towards O_2 for this MOF.

Conclusions

To this end, using periodic DFT calculations, we have shown that spin-state/exchange interaction plays a pivotal role in dictating gas adsorption selectivity in Cr MOF. Among the $O_2/N_2/H_2$ gases studied, the electron transfer mechanism adopted by O_2 leads to its strong spin-state dependent binding while the other two gases do not exhibit such drastic variations. As the O_2/N_2 selective adsorption/desorption process has high commercial value, this study offers a hitherto unknown strategy of utilizing spin-state/spin-couplings switching to control gas adsorption selectivity in MOFs.

Conflicts of interest

There are no conflicts to declare.

Acknowledgements

We thank DST and SERB (CRG/2018/000430; DST/SJF/CSA-03/2018-10; SB/SJF/2019-20/12). RJ thanks DST-INSPIRE for a fellowship. We thank Prof. Gagliardi, the University of Minnesota, for their help with the RASPA simulation.

References

1. (a) Mao, V. Y.; Milner, P. J.; Lee, J. H.; Forse, A. C.; Kim, E. J.; Siegelman, R. L.; McGuirk, C. M.; Porter-Zasada, L. B.; Neaton, J. B.; Reimer, J. A., Cooperative Carbon Dioxide Adsorption in Alcoholamine-and Alkoxyalkylamine-Functionalized Metal–Organic Frameworks. *Angew. Chem. Int. Ed.* **2020,** *59* (44), 19468-19477; (b) Kim, E. J.; Siegelman, R. L.; Jiang, H. Z.; Forse, A. C.; Lee, J.-H.; Martell, J. D.; Milner, P. J.; Falkowski, J. M.; Neaton, J. B.; Reimer, J. A., Cooperative carbon capture and steam regeneration with tetraamine-appended metal–organic frameworks. *Science* **2020,** *369* (6502), 392-396; (c) Connolly, B. M.; Madden, D. G.; Wheatley, A. E.; Fairen-Jimenez, D., Shaping the future of fuel: Monolithic metal–organic frameworks for high-density gas storage. *J. Am. Chem. Soc.* **2020,** *142* (19), 8541-8549; (d) Nagaraja, C.; Haldar, R.; Maji, T. K.; Rao, C., Chiral porous metal–organic frameworks of Co (II) and Ni (II): synthesis, structure, magnetic properties, and CO2 uptake. *Cryst. Growth Des.* **2012,** *12* (2), 975-981.
2. (a) Qian, Q.; Asinger, P. A.; Lee, M. J.; Han, G.; Mizrahi Rodriguez, K.; Lin, S.; Benedetti, F. M.; Wu, A. X.; Chi, W. S.; Smith, Z. P., MOF-based membranes for gas separations. *Chem. Rev.* **2020,** *120* (16), 8161-8266; (b) Liu, L.; Yao, Z.; Ye, Y.; Yang, Y.; Lin, Q.; Zhang, Z.; O'Keeffe, M.; Xiang, S., Integrating the Pillared-Layer Strategy and Pore-Space Partition Method to Construct Multicomponent MOFs for C2H2/CO2 Separation. *J. Am. Chem. Soc.* **2020,** *142* (20), 9258-9266; (c) Jaramillo, D. E.; Reed, D. A.; Jiang, H. Z.; Oktawiec, J.; Mara, M. W.; Forse, A. C.; Lussier, D. J.; Murphy, R. A.; Cunningham, M.; Colombo, V., Selective nitrogen adsorption via backbonding in a metal–organic framework with exposed vanadium sites. *Nat. Mater.* **2020,** *19* (5), 517-521; (d) Hou, Q.; Zhou, S.; Wei, Y.; Caro, J. r.; Wang, H., Balancing the Grain Boundary Structure and the Framework Flexibility through Bimetallic Metal–Organic Framework (MOF) Membranes for Gas Separation. *J. Am. Chem. Soc.* **2020,** *142* (21), 9582-9586; (e) Wang, H.; Shi, Z.; Yang, J.; Sun, T.; Rungtaweevoranit, B.; Lyu, H.; Zhang, Y. B.; Yaghi, O. M., Docking of CuI and AgI in Metal–Organic Frameworks for Adsorption and Separation of Xenon. *Angew. Chem. Int. Ed.* **2021,** *133* (7), 3459-3463; (f) Xu, W.; Yaghi, O. M., Metal–organic frameworks for water harvesting from air, anywhere, anytime. *ACS Cent. Sci.* **2020,** *6* (8), 1348-1354.
3. (a) Wang, X. Z.; Mao, X. Y.; Zhang, Z. Q.; Guo, R.; Zhang, Y. Y.; Zhu, N. J.; Wang, K.; Sun, P. P.; Huo, J. Z.; Wang, X. R., Solvothermal and Ultrasonic Preparation of Two Unique Cluster-Based Lu and Y Coordination Materials: Metal–Organic Framework-Based Ratiometric Fluorescent Biosensor for an Ornidazole and Ronidazole and Sensing Platform for a Biomarker of Amoeba Liver Abscess. *Inorg. Chem.* **2020,** *59* (5), 2910-2922; (b) Zhang, L.-T.; Zhou, Y.; Han, S.-T., The role of metal–organic framework in electronic sensors. *Angew. Chem. Int. Ed.* **2020**; (c) Li, J.; Yuan, S.; Qin, J. S.; Pang, J.; Zhang, P.; Zhang, Y.; Huang, Y.; Drake, H. F.; Liu, W. R.; Zhou, H. C., Stepwise Assembly of Turn-on Fluorescence Sensors in Multicomponent Metal–Organic Frameworks for in Vitro Cyanide Detection. *Angew. Chem. Int. Ed.* **2020,** *59* (24), 9319-9323; (d) Jayaramulu, K.; Narayanan, R. P.; George, S. J.; Maji, T. K., Luminescent microporous metal–organic framework with functional lewis basic sites on the pore surface: specific

sensing and removal of metal ions. *Inorg. chem.* **2012,** *51* (19), 10089-10091; (e) Cao, L.-A.; Yao, M.-S.; Jiang, H.-J.; Kitagawa, S.; Ye, X.-L.; Li, W.-H.; Xu, G., A highly oriented conductive MOF thin film-based Schottky diode for self-powered light and gas detection. *J. Mater. Chem. A* **2020,** *8* (18), 9085-9090.
4. (a) Dutta, S.; Kumari, N.; Dubbu, S.; Jang, S. W.; Kumar, A.; Ohtsu, H.; Kim, J.; Cho, S. H.; Kawano, M.; Lee, I. S., Highly mesoporous metal-organic frameworks as synergistic multimodal catalytic platforms for divergent cascade reactions. *Angew. Chem. Int. Ed.* **2020,** *132* (9), 3444-3450; (b) Tiburcio, E.; Greco, R.; Mon, M.; Ballesteros-Soberanas, J.; Ferrando-Soria, J. s.; López-Haro, M.; Hernández-Garrido, J. C.; Oliver-Meseguer, J.; Marini, C.; Boronat, M., Soluble/MOF-Supported Palladium Single Atoms Catalyze the Ligand-, Additive-, and Solvent-Free Aerobic Oxidation of Benzyl Alcohols to Benzoic Acids. *J. Am. Chem. Soc.* **2021,** *143* (6), 2581-2592; (c) Li, M.; Chen, J.; Wu, W.; Fang, Y.; Dong, S., Oxidase-like MOF-818 Nanozyme with High Specificity for Catalysis of Catechol Oxidation. *J. Am. Chem. Soc.* **2020,** *142* (36), 15569-15574; (d) Peralta, R. A.; Huxley, M. T.; Evans, J. D.; Fallon, T.; Cao, H.; He, M.; Zhao, X. S.; Agnoli, S.; Sumby, C. J.; Doonan, C. J., Highly Active Gas Phase Organometallic Catalysis Supported Within Metal–Organic Framework Pores. *J. Am. Chem. Soc.* **2020,** *142* (31), 13533-13543; (e) Jiang, Z.; Xu, X.; Ma, Y.; Cho, H. S.; Ding, D.; Wang, C.; Wu, J.; Oleynikov, P.; Jia, M.; Cheng, J., Filling metal–organic framework mesopores with TiO 2 for CO 2 photoreduction. *Nature* **2020,** *586* (7830), 549-554; (f) Trickett, C. A.; Popp, T. M. O.; Su, J.; Yan, C.; Weisberg, J.; Huq, A.; Urban, P.; Jiang, J.; Kalmutzki, M. J.; Liu, Q.; Baek, J., Head-Gordon,Martin P., Somorjai, Gabor A., Reimer, Jeffrey A., Yaghi, Omar M., , Identification of the strong Brønsted acid site in a metal–organic framework solid acid catalyst. *Nat. Chem.* **2019,** *11* (2), 170-176; (g) Baek, J.; Rungtaweevoranit, B.; Pei, X.; Park, M.; Fakra, S. C.; Liu, Y.-S.; Matheu, R.; Alshmimri, S. A.; Alshehri, S.; Trickett, C. A.; Somorjai Gabor A., Yaghi Omar M.,, Bioinspired metal–organic framework catalysts for selective methane oxidation to methanol. *J. Am. Chem. Soc.* **2018,** *140* (51), 18208-18216.
5. (a) Lin, R.-B.; Xiang, S.; Xing, H.; Zhou, W.; Chen, B., Exploration of porous metal–organic frameworks for gas separation and purification. *Coord. Chem. Rev.* **2019,** *378*, 87-103; (b) Li, H.; Wang, K.; Sun, Y.; Lollar, C. T.; Li, J.; Zhou, H.-C., Recent advances in gas storage and separation using metal–organic frameworks. *Mater. Today* **2018,** *21* (2), 108-121.
6. Haldar, R.; Maji, T. K., Metal–organic frameworks (MOFs) based on mixed linker systems: structural diversities towards functional materials. *CrystEngComm* **2013,** *15* (45), 9276-9295.
7. (a) Allendorf, M. D.; Foster, M. E.; Leonard, F.; Stavila, V.; Feng, P. L.; Doty, F. P.; Leong, K.; Ma, E. Y.; Johnston, S. R.; Talin, A. A., Guest-induced emergent properties in metal–organic frameworks. *J. Phys. Chem. Lett.* **2015,** *6* (7), 1182-1195; (b) Southon, P. D.; Liu, L.; Fellows, E. A.; Price, D. J.; Halder, G. J.; Chapman, K. W.; Moubaraki, B.; Murray, K. S.; Létard, J.-F.; Kepert, C. J., Dynamic interplay between spin-crossover and host− guest function in a nanoporous metal− organic framework material. *J. Am. Chem. Soc.* **2009,** *131* (31), 10998-11009.
8. (a) Wriedt, M.; Yakovenko, A. A.; Halder, G. J.; Prosvirin, A. V.; Dunbar, K. R.; Zhou, H.-C., Reversible switching from antiferro-to ferromagnetic behavior by solvent-mediated, thermally-induced phase transitions in a trimorphic MOF-based magnetic sponge system. *J. Am. Chem. Soc.*

2013, *135* (10), 4040-4050; (b) Park, J.; Yuan, D.; Pham, K. T.; Li, J.-R.; Yakovenko, A.; Zhou, H.-C., Reversible alteration of CO2 adsorption upon photochemical or thermal treatment in a metal–organic framework. *J. Am. Chem. Soc.* **2012,** *134* (1), 99-102.
9. Yuan, S.; Sun, X.; Pang, J.; Lollar, C.; Qin, J.-S.; Perry, Z.; Joseph, E.; Wang, X.; Fang, Y.; Bosch, M., PCN-250 under pressure: sequential phase transformation and the implications for MOF densification. *Joule* **2017,** *1* (4), 806-815.
10.Kather, A.; Scheffknecht, G., The oxycoal process with cryogenic oxygen supply. *Naturwissenschaften* **2009,** *96* (9), 993-1010.
11.Li, J.-R.; Kuppler, R. J.; Zhou, H.-C., Selective gas adsorption and separation in metal–organic frameworks. *Chem. Soc. Rev.* **2009,** *38* (5), 1477-1504.

12.Bloch, E. D.; Queen, W. L.; Hudson, M. R.; Mason, J. A.; Xiao, D. J.; Murray, L. J.; Flacau, R.; Brown, C. M.; Long, J. R., Hydrogen storage and selective, reversible O2 adsorption in a metal–organic framework with open chromium (II) sites. *Angew. Chem. Int. Ed.* **2016,** *55* (30), 8605-8609.
13.(a) Xianyu, Y.; Dong, Y.; Zhang, Z.; Wang, Z.; Yu, W.; Wang, Z.; Chen, Y., Gd3+-nanoparticle-enhanced multivalent biosensing that combines magnetic relaxation switching and magnetic separation. *Biosens. Bioelectron.* **2020,** *155*, 112106; (b) Hu, Y.; Guo, X.; Wang, H.; Luo, Q.; Song, Y.; Song, E., Magnetic-Separation-Assisted Magnetic Relaxation Switching Assay for Mercury Ion Based on the Concentration Change of Oligonucleotide-Functionalized Magnetic Nanoparticle. *ACS Appl. Bio Mater.* **2020,** *3* (5), 2651-2657.
14.Kosaka, W.; Liu, Z.; Zhang, J.; Sato, Y.; Hori, A.; Matsuda, R.; Kitagawa, S.; Miyasaka, H., Gas-responsive porous magnet distinguishes the electron spin of molecular oxygen. *Nat. Commun* **2018,** *9* (1), 1-9.
15.Nazarian, D.; Ganesh, P.; Sholl, D. S., Benchmarking density functional theory predictions of framework structures and properties in a chemically diverse test set of metal–organic frameworks. *J. Mater. Chem. A* **2015,** *3* (44), 22432-22440.
16.Harvey, J. N., On the accuracy of density functional theory in transition metal chemistry. *Annu. Rep. Prog. Chem., Sect. C: Phys. Chem.* **2006,** *102*, 203-226.
17.Nabi, R.; Rajaraman, G., Deciphering the origin of variation in the spin ground state and oxidation state of a {Mn 19} cluster on a Au (111) surface: is the Au (111) surface innocent? *Chemical Communications* **2019,** *55* (57), 8238-8241.
18.Ruiz, E.; Cauchy, T.; Cano, J.; Costa, R.; Tercero, J.; Alvarez, S., Magnetic structure of the large-spin Mn10 and Mn19 complexes: a theoretical complement to an experimental milestone. *J. Am. Chem. Soc.* **2008,** *130* (23), 7420-7426.
19.Dubbeldam, D.; Calero, S.; Ellis, D. E.; Snurr, R. Q., RASPA: molecular simulation software for adsorption and diffusion in flexible nanoporous materials. *Molecular Simulation* **2016,** *42* (2), 81-101.
20.Rappé, A. K.; Casewit, C. J.; Colwell, K.; Goddard III, W. A.; Skiff, W. M., UFF, a full periodic table force field for molecular mechanics and molecular dynamics simulations. *Journal of the American chemical society* **1992,** *114* (25), 10024-10035.
21.Potoff, J. J.; Siepmann, J. I., Vapor–liquid equilibria of mixtures containing alkanes, carbon dioxide, and nitrogen. *AIChE journal* **2001,** *47* (7), 1676-1682.
22.(a) Schwalbe, S.; Trepte, K.; Seifert, G.; Kortus, J., Screening for high-spin metal organic frameworks (MOFs): density functional theory study on DUT-8 (M 1, M 2)(with M i= V,…, Cu). *Phys. Chem. Chem. Phys.* **2016,** *18* (11), 8075-8080; (b) Odoh, S. O.; Cramer, C. J.; Truhlar, D. G.; Gagliardi, L., Quantum-chemical characterization of the properties and reactivities of metal–organic frameworks. *Chem. Rev.* **2015,** *115* (12), 6051-6111.
23.Ansari, A.; Jayapal, P.; Rajaraman, G., C□ H Bond Activation by Metal–Superoxo Species: What Drives High Reactivity? *Angew. Chem. Int. Ed.* **2015,** *127* (2), 574-578.
24.Ruiz, E.; Cano, J.; Alvarez, S.; Alemany, P., Broken symmetry approach to calculation of exchange coupling constants for homobinuclear and heterobinuclear transition metal complexes. *J. Comput. Chem.* **1999,** *20* (13), 1391-1400.
25.Fryzuk, M. D.; Leznoff, D. B.; Rettig, S. J.; Thompson, R. C., Magnetic Exchange in Dinuclear Chromium (II) Complexes: Effect of Bridging Chlorides and Bridging Hydrides in Antiferromagnetic Coupling. *Inorg. chem.* **1994,** *33* (24), 5528-5534.
26.Cho, J.; Woo, J.; Nam, W., An "End-On" chromium (III)-superoxo complex: crystallographic and spectroscopic characterization and reactivity in C− H bond activation of hydrocarbons. *J. Am. Chem. Soc.* **2010,** *132* (17), 5958-5959.
27.Rosen, A. S.; Mian, M. R.; Islamoglu, T.; Chen, H.; Farha, O. K.; Notestein, J. M.; Snurr, R. Q., Tuning the Redox Activity of Metal–Organic Frameworks for Enhanced, Selective O2 Binding: Design Rules and Ambient Temperature O2 Chemisorption in a Cobalt–Triazolate Framework. *J. Am. Chem. Soc.* **2020,** *142* (9), 4317-4328.

TOC text: The importance of spin-state and spin-coupling in gas binding selectivity in MOFs are uncovered using periodic DFT calculations.